The Journal of Chemical Physics

RESEARCH ARTICLE | JULY 17 2023

A modeling approach to understanding OLED performance improvements arising from spatial variations in guest:host blend ratio

M. Greenberg ; S. Sanderson ; R. D. White ; G. Vamvounis ; P. L. Burn ; B. Philippa

J. Chem. Phys. 159, 034101 (2023)
https://doi.org/10.1063/5.0152922

The Journal of Chemical Physics ARTICLE pubs.aip.org/aip/jcp

A modeling approach to understanding OLED performance improvements arising from spatial variations in guest:host blend ratio

Cite as: J. Chem. Phys. 159, 034101 (2023); doi: 10.1063/5.0152922
Submitted: 3 April 2023 • Accepted: 27 June 2023 •
Published Online: 17 July 2023

M. Greenberg,[1] S. Sanderson,[1] R. D. White,[1] G. Vamvounis,[1] P. L. Burn,[2] and B. Philippa[1,a)]

AFFILIATIONS

[1] College of Science and Engineering, James Cook University, Townsville QLD 4811, Australia
[2] Centre for Organic Photonics and Electronics, School of Chemistry and Molecular Biosciences, The University of Queensland, Brisbane QLD 4072, Australia

[a)] **Author to whom correspondence should be addressed:** bronson.philippa@jcu.edu.au

ABSTRACT

Phosphorescent organic light emitting diodes (OLEDs) suffer from efficiency roll off, where device efficiency rapidly decays at higher luminance. One strategy to minimize this loss of efficiency at higher luminance is the use of non-uniform or graded guest:host blend ratios within the emissive layer. This work applies a multi-scale modeling framework to elucidate the mechanisms by which a non-uniform blend ratio can change the performance of an OLED. Mobility and exciton data are extracted from a kinetic Monte–Carlo model, which is then coupled to a drift diffusion model for fast sampling of the parameter space. The model is applied to OLEDs with uniform, linear, and stepwise graduations in the blend ratio in the emissive layer. The distribution of the guests in the film was found to affect the mobility of the charge carriers, and it was determined that having a graduated guest profile broadened the recombination zone, leading to a reduction in second order annihilation rates. That is, there was a reduction in triplet–triplet and triplet-polaron annihilation. Reducing triplet–triplet and triplet-polaron annihilation would lead to an improvement in device efficiency.

INTRODUCTION

Phosphorescent organic light emitting diodes (OLEDs) generally show a roll-off in efficiency with increasing luminance.[1,2] At higher luminance, the non-radiative losses increase and, consequently, the overall device performance declines. To address this problem of roll-off, it is important to understand the processes of excited state (exciton) decay. Phosphorescent emitters can utilize both the singlet and triplet excited states generated in the device, with singlets undergoing intersystem crossing to yield triplets, which in turn can decay radiatively. The most efficient phosphorescent OLEDs have the emitter material blended into a host material with the goal of increasing the distance between emitters and, hence, reducing the detrimental intermolecular interactions that can lead to exciton quenching. In working devices, these can include triplet–triplet annihilation (TTA) and triplet-polaron quenching (TPQ).[3–5]

Triplet–triplet annihilation is a process in which two triplet excitons interact, leading to the formation of an excited singlet or triplet, governed through spin statistics, with the other returning to the ground state. If the singlet is formed on a phosphorescent chromophore, it can intersystem cross back to the triplet state. Triplet-polaron quenching is a process in which a triplet interacts with a polaron, which leads to the triplet decaying non-radiatively to the ground state.[2] Since these processes are bimolecular, a large density of polarons or excitons within a region of the emissive layer can increase the probability of TTA or TPQ occurring. That is, the degree of TTA and TPQ that occurs within a phosphorescent emissive film is dependent on the distribution of the emitter molecules in the blend film and/or the recombination zone (the region of the film in which holes and electrons recombine). For example, clustering of the emitters could lead to increased TTA, while unbalanced charge transport within the device could lead to the accumulation of excitons and polarons at an interface, thereby increasing TPQ.

One strategy to decrease the impact of these exciton loss mechanisms is via control of the recombination zone, since a broadening of this zone will reduce charge carrier/exciton accumulation and, in particular, limit TPQ.[6] There have been a number of reports showing a reduction in efficiency roll-off by introducing a guest:host blend ratio gradient in the emissive layer normal to the substrate.[6–12] For example, one study by Zhang *et al.* attributed improved device efficiency and lifetime to the use of a linearly graded guest:host blend ratio.[6] In that study, the guest concentration was highest near the hole transport layer (HTL) and declined linearly through the film. They attributed the improvement to variations in hole transport within the emissive layer, which decreased with increasing distance from the HTL, thus reducing charge accumulation at the electron injection/hole blocking interface. In another study, Chin *et al.* also observed a similar effect for devices in which the concentration of the guest was changed in a stepwise fashion by sequentially depositing layers having different guest:host ratios.[9] Interestingly, it was found that the highest guest concentration should be near the HTL for one material blend and near the electron transport layer (ETL) for a different blend, with the optimal design depending on the material and device properties.

It is important to note that while these approaches can control the average vertical distribution of the emitter materials in the emissive layers, their distribution in the plane of the substrate is generally unknown with atomic resolution. Indeed, molecular dynamics simulations show that even under ideal deposition conditions, emitters are not evenly distributed throughout the emissive layer, and even at relatively low emitter concentrations in a host, there can be interconnected pathways for exciton and polaron migration.[13,14]

While the reported experimental results have shown that nonuniform guest:host blend ratios in the emissive layer can increase device performance, there are fewer simulation studies aimed at identifying the underlying reason for the improvement in performance.[7] Notably, the large variation in material combinations and device architectures means that it is difficult to systematically address the underlying mechanisms that lead to the improvement in performance.

In this paper, we seek to understand the detailed mechanism by which performance improvement is realized for different device scenarios. We employ a multi-scale modeling approach in which a microscopic model [kinetic Monte–Carlo (KMC)] is coupled to a macroscopic model (drift diffusion). The simulations are based on a prototypical phosphorescent OLED device structure,[15] with a HTL of *N*,*N*′-diphenyl-*N*,*N*′-*bis*(1-napthylphenyl)-1,1′-biphenyl-4,4′-diamine (*α*NPD), an emissive (EML) guest:host blend of *fac*-tris(2-phenylpyridine)iridium(III):4,4′-bis(*N*-carbazolyl)-1,1′-biphenyl [Ir(ppy)$_3$:CBP], a hole blocking layer (BL) of bathocuproine (BCP), and an electron transport layer (ETL) of tris(8-hydroxyquinoline)aluminum(III) (Alq$_3$) (Fig. 1). The layer thicknesses were 30, 30, 10, and 40 nm for the HTL, EML, BL, and ETL, respectively. The choice of these materials and device architectures was based on the fact that many of the parameters required for the simulations have been experimentally determined. Three device architectures were considered, which differed in the distribution of the emitter in the emissive layer. First, as shown in Fig. 1(a), we considered an EML that has a uniform guest:host blend ratio normal to the substrate, which represents the baseline for comparison. Second, we investigated an EML that was composed of two separate layers of equal thickness containing different blend ratios [Fig. 1(b)]. Finally, we explored an emissive layer that has a linear graduation in the blend ratio [Fig. 1(c)]. We will demonstrate how an optimal blend ratio configuration can be modeled for a given material system.

METHODOLOGY

Computational modeling

We used a multi-scale modeling approach, combining both KMC and drift-diffusion (DD) simulations.[16–19] We have previously published KMC simulations of Ir(ppy)$_3$:CBP films containing 2, 6, 10, 15, and 20 wt. % of Ir(ppy)$_3$ as well as neat films of the host.[16] In the previous work, it was assumed that the Ir(ppy)$_3$ molecules were on average evenly distributed through the bulk of the film, following a uniform random distribution [similar to Fig. 1(a)]. Since the KMC simulations are computationally expensive, we obtained estimates of the charge transport properties at intermediate values by interpolation of the discrete data points from previously published data,[16,17] as shown in Fig. 2. The properties that were considered to vary with blend ratio were electron and hole mobility and the yield of triplets, i.e., the proportion of excitons formed by electron–hole recombination that successfully diffuse to a guest molecule and undergo intersystem crossing to become triplets.

These data were provided as input into a drift-diffusion model. The drift-diffusion model allows for blend ratio variation across the active layer. The model, which describes the whole device, including transport layers, is given by Eqs. (1)–(7),

$$\frac{\partial p}{\partial t} + \frac{1}{e}\frac{\partial j_p}{\partial x} = -\beta np, \tag{1}$$

$$\frac{\partial n}{\partial t} - \frac{1}{e}\frac{\partial j_n}{\partial x} = -\beta np, \tag{2}$$

$$j_p(x,t) = e\mu_p(x,\rho_G)E(x,t)p(x,t) - \mu_p(x,\rho_G)k_BT\frac{\partial p}{\partial x}, \tag{3}$$

$$j_n(x,t) = e\mu_n(x,\rho_G)E(x,t)n(x,t) + \mu_n(x,\rho_G)k_BT\frac{\partial n}{\partial x}, \tag{4}$$

$$\frac{\partial^2 V}{\partial x^2} = \frac{n-p}{\varepsilon_r\varepsilon_0}, \tag{5}$$

$$E = -\frac{\partial V}{\partial x}, \tag{6}$$

$$\frac{\partial T_G}{\partial t} = k_{GEF}(\rho_G)\beta np - k_T\rho_G T_G - k_{Tnr}\rho_G T_G - k_{TTA}T_G{}^2 - k_{TPA}T_G(n+p) + \frac{\partial}{\partial x}\left(D_T\frac{\partial T_G}{\partial x}\right). \tag{7}$$

The guest concentration is defined as ρ_G, and the parameters that depend upon this concentration are labeled with an explicit dependence on ρ_G. Equations (1) and (2) are the charge continuity equations for holes and electrons, respectively, where $p(n)$ represents the

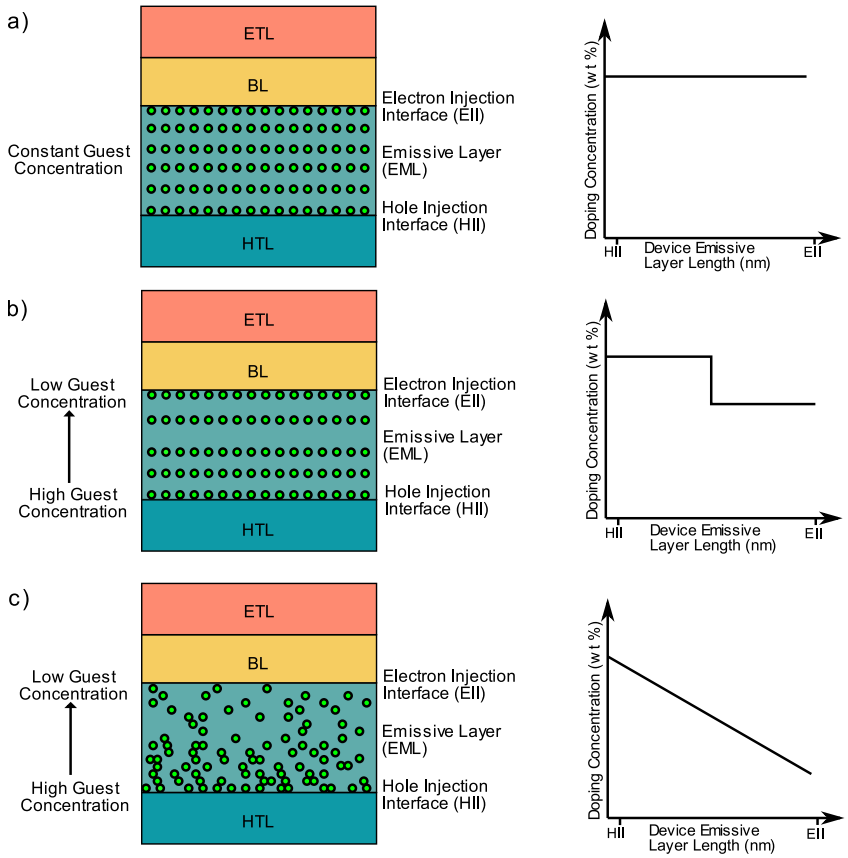

FIG. 1. Visual representations of the three device structures explored in this paper. Each structure consists of a hole transport layer (HTL), an emissive layer (EML), a blocking layer (BL), and an electron transport layer (ETL). The blocking layer also functions as an ETL. In the EML, the guest concentration varies from being (a) uniform, (b) having a stepwise change in the middle of the layer, and (c) having a linear gradient across the entire active layer normal to the substrate.

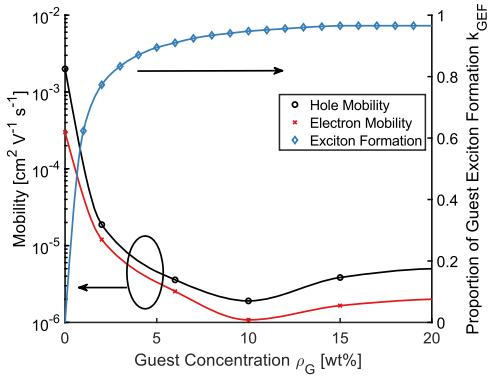

FIG. 2. Concentration-dependent mobility and exciton formation data obtained using kinetic Monte–Carlo simulations. The exciton formation data gives the proportion of recombining electron–hole pairs that either form directly on the guest or form on the host and diffuse to the guest. These data are used as input to the drift-diffusion model.

number density of holes (electrons) as a function of the distance, x, from the substrate and time, t, $j_{p(n)}$ is the hole (electron) current density, and β is the recombination coefficient. Equations (3) and (4) give the current density $j_{p(n)}$ for holes (electrons), where $\mu_{p(n)}(x, \rho_G)$ are the hole (electron) mobilities, respectively. The mobilities are a function of position x, which is used to represent the mobilities of each layer in the device. Within the active layer, mobility is also a function of guest concentration, ρ_G, as shown in Fig. 2. $E(x,t)$ gives the electric field, and the scalar values e, k_B, and T denote the electron charge, Boltzmann constant, and temperature, respectively. The Einstein relation for the diffusion coefficient has been assumed in Eqs. (3) and (4).

Next, Eqs. (5) and (6) denote the voltage (V) and electric field within the device, respectively. The voltages at the electrodes are held at a fixed value. The scalar values ε_r and ε_0 are the relative and vacuum permittivity, respectively.

Finally, Eq. (7) specifies the continuity equation for triplets within the emissive layer, where T_G is the time- and position dependent number density of triplets on the guest. Due to the large

TABLE I. Model parameters.

Parameter	Symbol	Value	References
αNPD hole mobility[a]	$\mu_{h\text{-}\alpha NPD}$	3.22×10^{-3} cm^2 V^{-1} s^{-1}	23
αNPD electron mobility	$\mu_{e\text{-}\alpha NPD}$	0 cm^2 V^{-1} s^{-1}	⋯
CBP hole mobility	$\mu_{h\text{-}CBP}$	2×10^{-3} cm^2 V^{-1} s^{-1}	24
CBP electron mobility	$\mu_{e\text{-}CBP}$	3×10^{-4} cm^2 V^{-1} s^{-1}	
BCP electron mobility	$\mu_{e\text{-}BCP}$	5.5×10^{-6} cm^2 V^{-1} s^{-1}	25
BCP hole mobility	$\mu_{h\text{-}BCP}$	0 cm^2 V^{-1} s^{-1}	⋯
Alq_3 electron mobility[a]	μ_{e-Alq_3}	4.3×10^{-6} cm^2 V^{-1} s^{-1}	26 and 27
Alq_3 hole mobility	μ_{h-Alq_3}	0 cm^2 V^{-1} s^{-1}	⋯
Relative permittivity	ε_r	2	16
Intersystem crossing rate	k_{isc}	6.9×10^{12} s^{-1}	28
Triplet–triplet annihilation rate	k_{TTA}	3×10^{-12} cm^3 s^{-1}	4 and 29
Triplet-polaron annihilation rate	k_{TPA}	2×10^{-13} cm^3 s^{-1}	4
Triplet diffusion length	L_D	6.8×10^{-9} m	21
Temperature	T	300 K	⋯

[a]The reference's Poole–Frenkel mobility was evaluated at an electric field of 1×10^6 V cm^{-1}.

TABLE II. Guest concentration dependent parameters. Radiative and non-radiative decay rates, which are provided as a function of guest concentration. Data from Ref. 14.

Guest concentration (wt. %)	Triplet radiative decay rate k_T (s^{-1})	Triplet non-radiative decay rate k_{Tnr} (s^{-1})
1	$7.59\ (\pm 0.44) \times 10^5$	$1.84\ (\pm 0.44) \times 10^5$
6	$7.54\ (\pm 0.44) \times 10^5$	$1.39\ (\pm 0.44) \times 10^5$
10	$6.83\ (\pm 0.40) \times 10^5$	$1.94\ (\pm 0.40) \times 10^5$
20	$5.82\ (\pm 0.35) \times 10^5$	$3.61\ (\pm 0.35) \times 10^5$
50	$5.91\ (\pm 0.40) \times 10^5$	$6.91\ (\pm 0.40) \times 10^5$

intersystem crossing rate of $Ir(ppy)_3$, it is assumed that all singlets that form either directly on the guest or diffuse to a guest molecule immediately undergo intersystem crossing to become triplets. The proportion of excitons reaching a guest molecule was obtained from the KMC simulations, as plotted in Fig. 2. These values appear in the drift-diffusion model as a yield parameter for guest exciton formation, k_{GEF}. Since we assume a very fast intersystem crossing rate, all excitons reaching the guest are considered to instantaneously become triplets and, therefore, singlet excitons are not modeled. This is an approximation which assumes that the concentration of singlets is much less than the concentration of triplets.[20] For Eq. (7), $k_{Tr}(\rho_G)$ and $k_{Tnr}(\rho_G)$ are the radiative and non-radiative triplet decay rates, respectively, which are a function of guest concentration. These values were sourced from experimental measurements utilizing Photoluminescence Quantum Yield (PLQY) and triplet lifetimes, which are published in the literature.[14] k_{TTA} is the triplet–triplet annihilation rate, and k_{TPQ} is the triplet polaron annihilation rate. The triplet diffusion coefficient D_T was calculated through the relation $L_D = \sqrt{6 D_T \tau_D}$, where L_D is the measured three dimensional diffusion length and τ_D is the measured triplet lifetime.[21]

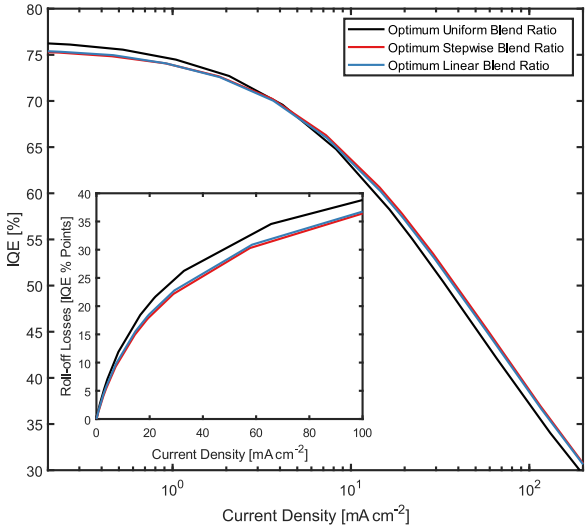

FIG. 3. Internal quantum efficiency (IQE) as a function of current density for optimum devices with uniform, stepwise, and linear graded EMLs. The non-uniform doping profiles show an improvement in IQE. The inset shows the roll-off losses calculated from the same data, where the roll-off loss is defined as the difference between the maximum IQE and the IQE at the given current density.

To further constrain the number of parameters in the model, we have assumed that there is no energetic barrier to electron and hole injection from a transport layer into the emissive layer, and all particles (holes, electrons, and excitons) within the EML are assumed to be confined there. As a result of these assumptions, charge carrier energy levels were not included as input parameters. Furthermore, we have assumed ideal ohmic charge injection, which we define to be where charges rapidly inject until the electric field

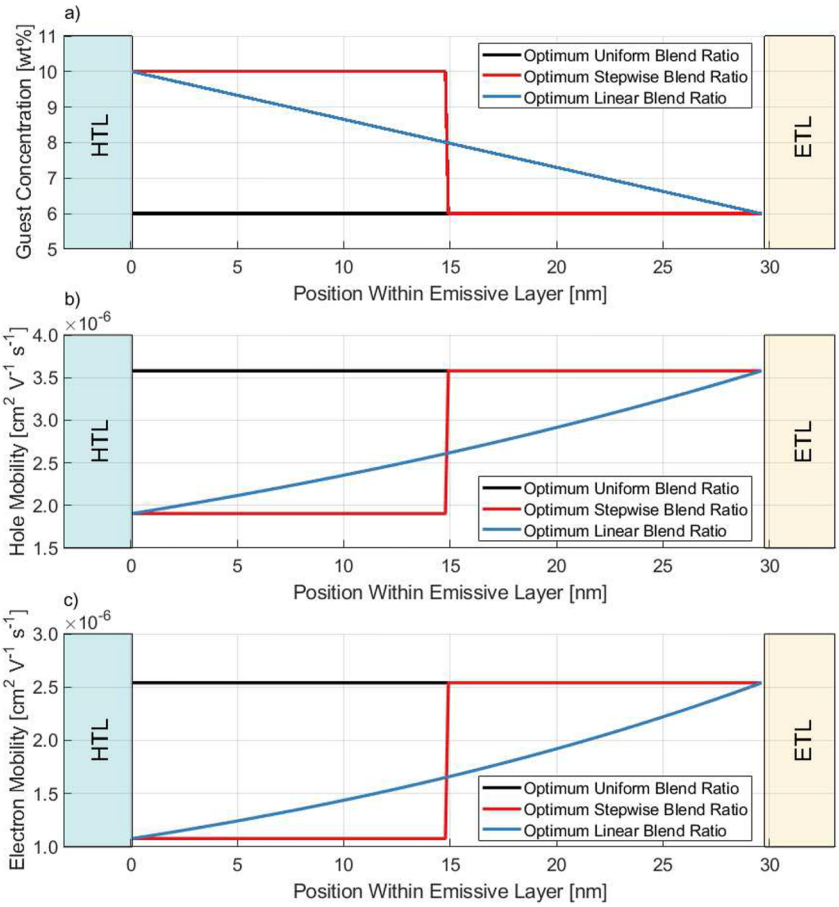

FIG. 4. (a) Visual representation of the optimal blend ratio distribution for devices with uniform, stepwise, and linear EML blends. In addition, shown are the resulting (b) hole and (c) electron mobilities. HTL refers to the hole transport layer, and ETL refers to the hole blocking layer and electron transport layer.

at the interface is completely screened.[22] This ensures that our simulated devices are always operating in the regime of space-charge-limited current. Other material properties, such as the mobilities in the transport layers and the exciton rate constants, were sourced from the literature. The parameters used in the model are given in Tables I and II.

RESULTS

Figure 3 shows the internal quantum efficiencies (IQEs) of the highest performing devices with uniform, stepwise, or linear blend EMLs. These optimum configurations were found through an exhaustive search of all possible blend ratio configurations in increments of 1 wt. %. The optimum blend ratio configuration for the linear device was a concentration of $Ir(ppy)_3$ that linearly decreased from 10 wt. % at the hole-injecting interface (HII) to 6 wt. % at the electron-injecting interface (EII). For the stepwise device, the same concentrations of 10 and 6 wt. % at HII and EII, respectively, were also optimal. For the uniform device, the optimum concentration was 6 wt. %, aligning with the reported experimental results.[30] As is evident, the two non-uniform devices exhibit performance improvements and a reduction in roll-off, as plotted in the inset in Fig. 3. Both linear and stepwise EML blends exhibit an overall reduction in roll-off that improves with increasing current density. This shows that non-uniform blend ratios can provide a performance benefit. It is also important to note that the stepwise blend profile in the EML, which is far simpler to fabricate, is just as effective as the linear profile.

We note that at low current densities, the non-uniform blend ratios in the EML lead to a reduction in IQE compared to a device with a uniform EML. At low current densities, the primary loss mechanisms are the non-radiative decay of triplets on the guest and the loss of excitons that form on the host but do not transfer to the guest. In this regime, the increase in doping concentration for the two devices with non-uniform EMLs leads to an increase in non-radiative decay, as presented in Table II, resulting in an overall increase in triplets lost non-radiatively.[14] At a current density of ~6 mA cm^{-2}, triplet density becomes significant, and second order annihilation (TTA and TPQ) become the primary loss mechanisms, driving the efficiency roll-off losses. As such, devices with

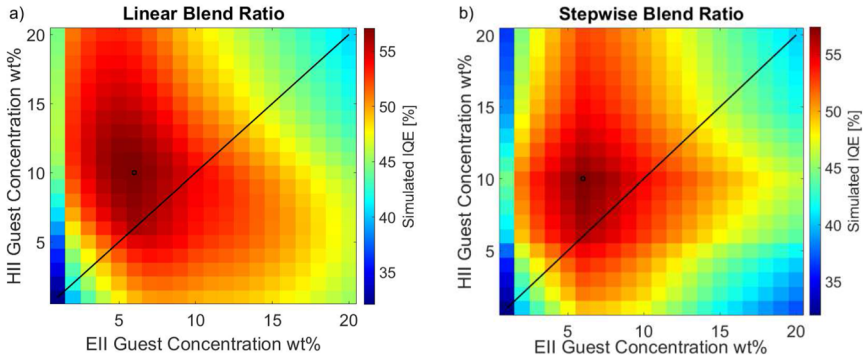

FIG. 5. Internal quantum efficiency (IQE) for the varying guest:host blend ratios, where the blend ratio in the EML changes (a) linearly and (b) in a step. The horizontal and vertical axes indicate the guest concentration at the hole-injecting interface (HII) and electron-injecting interface (EII), respectively (Please refer to Fig. 1 for the interpretation of these interface layers and the resulting blend profiles). The solid black line indicates a uniform blend ratio. The highest IQE is indicated with a small black circle at 6 wt. % at the EII and 10 wt. % at the HII for both (a) and (b). These two circles represent the optimal linear and stepwise EML blends that were shown in Fig. 3.

non-uniform EMLs driven at higher current densities begin to show a benefit.

Figure 4 depicts the blend ratio distributions for the optimal devices whose performance was shown in Fig. 3. The figure also shows the hole and electron mobilities that result from these blend ratios. As is evident, the introduction of a higher guest concentration at the hole-injecting interface leads to an approximate halving of both the electron and hole mobilities, which arises from the fact that the $Ir(ppy)_3$ guests act as charge traps in the CBP host.

Figure 5 shows the predicted performance across the design space of all possible linear and stepwise blend ratio configurations for the EML. In particular, the heatmaps show the predicted IQE at a constant current density of 20 mA cm^{-2}, which in similar devices was measured to correspond to an approximate luminance of 3500 cd m^{-2}.[31] It is evident that there is a region of non-uniform guest distribution within the host that exhibits an increased IQE for both linear and stepwise EML profiles. Furthermore, the EML with a linear distribution of the emissive guest in the host has a wider zone of improved device performance, which indicates a potential for robustness in device performance against variations that can arise during manufacturing.

To understand the mechanism of performance improvement, these optimum devices were investigated in more detail. Figure 6 shows the recombination rate and charge carrier densities for the three optimum device configurations. We note large hole accumulation at the electron injection interface and a low concentration of electrons across the EML, which can be attributed to the strong mobility imbalance of the transport and emissive layers.

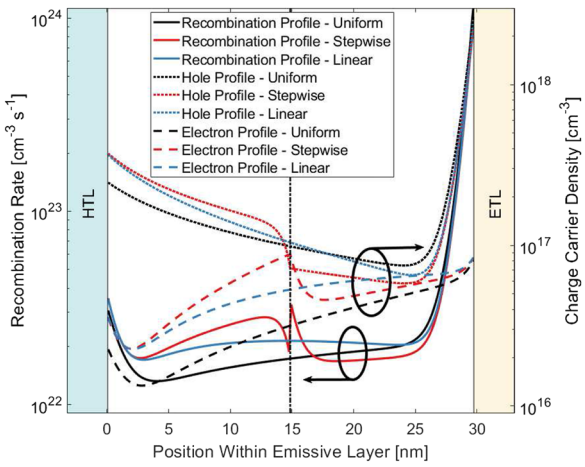

FIG. 6. Spatial profile of charge carrier recombination rate (calculated as βnp) (LHS) and charge carrier density (RHS) for three different EML types. A discontinuity in the recombination rate can be observed at the interface, where the guest concentration undergoes a stepwise change, which is shown with the vertical dotted line at 15 nm. The consistent charge carrier injection for the three devices ensures an equal exciton generation rate.

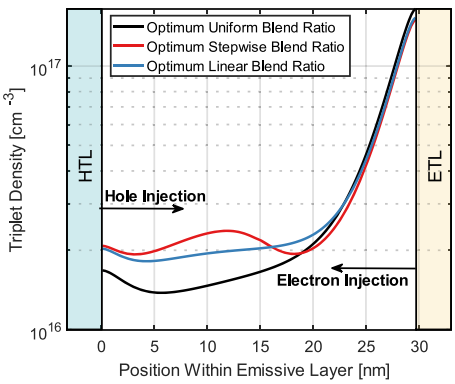

FIG. 7. Spatial profile of triplet concentration within the EML for three sampled devices at a steady state current density of 20 mA cm^{-2} (which corresponds to an approximate luminance of 3500 cd m^{-2}). The optimal profiles show a broadened and more uniform concentration of triplets, especially toward the middle of the layer.

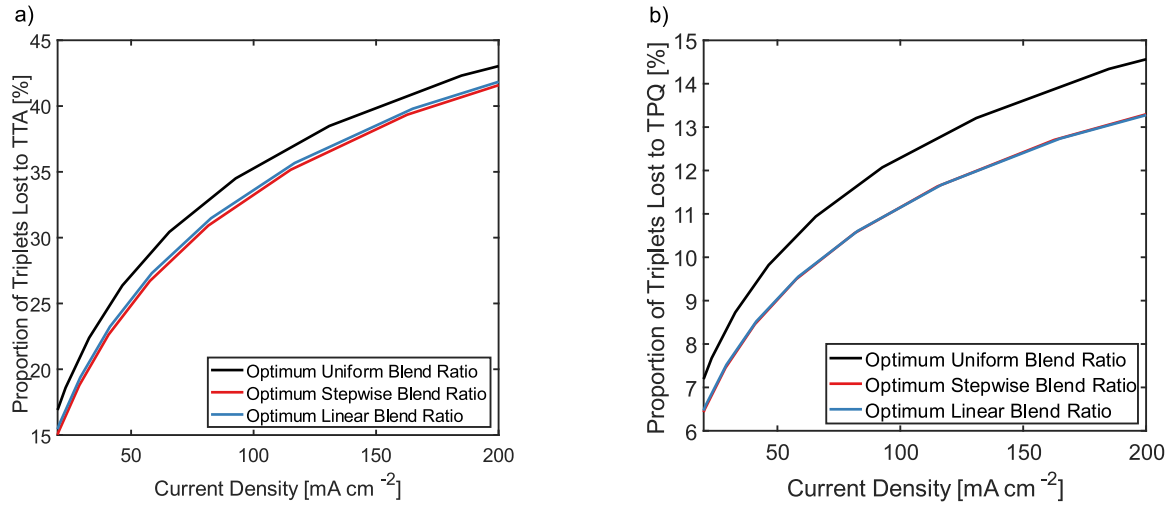

FIG. 8. Proportional loss of triplets due to (a) triplet–triplet annihilation (TTA) and (b) triplet-polaron quenching (TPQ) as a function of current density for three sampled devices. The graph clearly shows a reduction in loss processes for the two devices with non-uniform EMLs.

The simulated devices with non-uniform EMLs show an increased spread of both hole and electron (Fig. 6) and triplet (Fig. 7) concentrations throughout the EML, which is directly reflected in the broadening of the recombination zone. We attribute this behavior to a blend-ratio-induced decrease in hole mobility across the EML, with the strongest effect at the hole injection interface, which counteracts the mobility mismatch between the transport layers. The higher blend ratio corresponds to increased charge carrier trapping on the $Ir(ppy)_3$ guest molecules, reducing the mobility in that region. In this way, a targeted decrease in mobility can lead to improved device performance by compensating for imbalances elsewhere.

To directly examine the loss mechanisms, Figs. 8(a) and 8(b) show the percentage losses of triplets due to TTA and TPQ across a range of current densities. There is a clear reduction in these loss mechanisms in devices containing a non-uniform blend ratio in the EML.

These results clearly indicate that the devices with non-uniform EMLs performed better because they improved the mobility balance. However, there are several ways that mobility balance can be defined. There is a balance between hole and electron mobility within the EML, but there is also a balance between the hole mobility in the HTL and the electron mobility in the ETL.

The time-dependence of the turn-on process (video in the supplementary material) was examined, and it was observed that the "wave fronts" of injecting holes and electrons first make contact near the edge of the ETL. Hence, it is likely that the HTL/ETL imbalance (not the EML imbalance) is most critical in these devices. A consequence of this proposition is that if the relative mobilities were swapped so that electrons in the ETL had faster mobility, our analysis would lead to a mirror reflection of the heatmaps (Fig. 5) about the diagonal line. That is, the highest guest concentration should be at the electron-injecting interface instead of the hole-injecting interface. To test whether the analysis was correct, we simulated a mirrored device with the resulting structure of HTL/BL/EML/ETL. The mobilities were mirrored such that the original HTL hole mobility became the new ETL electron mobility (and vice versa). The blocking layer was swapped to the other side of the device, and its electron and hole mobilities were swapped. In essence, this device has an identical EML, but the charge transport properties of the transport layers are swapped so that electrons have faster transport. The results of these simulations are shown

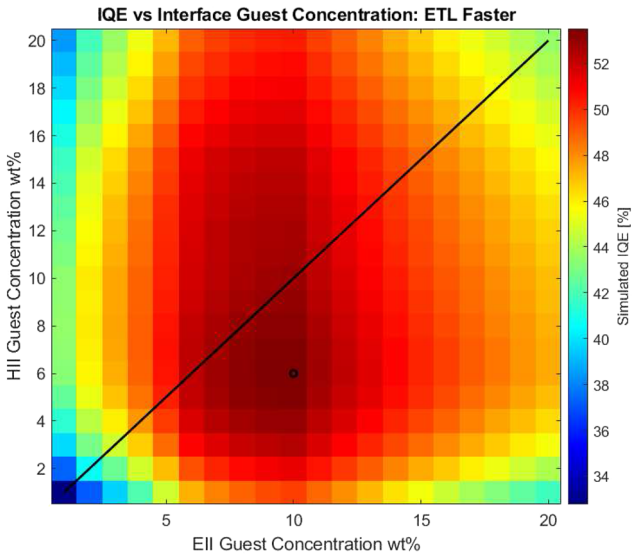

FIG. 9. Performance of a "mirrored" device configuration where the mobilities of electrons and holes in the transport layers are swapped such that the electron transport layer is faster than the hole transport layer. In comparison to Fig. 5(b), there is approximately a mirror reflection in the overall heatmap. Hence, it is the mobility in the transport layers that critically determines how the profile of the guest in the EML should be optimized.

in Fig. 9. Notably, this heatmap is indeed close to a mirror reflection of Fig. 5. This confirms that the mobility imbalance in the transport layers is also a critical factor in determining the optimum guest profile in the EML, at least for the materials and geometries studied here.

CONCLUSION

In this paper, we have examined how non-uniform blend ratios of guest and host materials can improve performance in a prototypical $Ir(ppy)_3$:CBP OLED system. Kinetic Monte–Carlo modeling highlighted that varying the profile of the blend ratio has a large impact on the carrier's mobility. Multi-scale modeling found that an imbalance in transport layer charge mobilities of the studied devices containing $Ir(ppy)_3$:CBP emissive layer blends resulted in an accumulation of holes at the electron-injecting interface of the emissive layer, restricting the recombination zone and maximizing exciton losses. By increasing the blend ratio at the hole-injecting interface of the emissive layer, the hole mobility could be effectively tuned and some mobility balance restored. The resultant devices with non-uniform EMLs showed increased device performance. This behavior was attributed to a broadening of the recombination zone, which was a direct consequence of the effective grading of the hole mobility. Consequently, careful tuning of the spatial profile of the blend ratio can minimize losses due to triplet–triplet annihilation and triplet-polaron quenching. This study has highlighted the potential benefits that can be realized through non-uniform guest:host blend ratios within the emissive layer. However, maximizing efficiency was found to be dependent on the emissive layer structure as well as the relative charge mobilities in the transport layers.

SUPPLEMENTARY MATERIAL

See the supplementary material for a video showing the electron and hole densities in the device during the turn-on process, as referred to in the main text.

ACKNOWLEDGMENTS

We wish to acknowledge the computational resources provided by the James Cook University High Performance Computing Facilities. M.G. was supported by an Australian Government Research Training Program Scholarship. This research was supported, in part, by the Australian Government through an Australian Research Council Discovery Project (Grant No. DP210102192). P.L.B. was an ARC Laureate Fellow (Grant No. FL160100067).

AUTHOR DECLARATIONS

Conflict of Interest

The authors have no conflicts to disclose.

Author Contributions

M. Greenberg: Conceptualization (equal); Software (equal); Validation (equal); Visualization (equal); Writing – original draft (equal); Writing – review & editing (equal). **S. Sanderson**: Software (equal); Writing – review & editing (equal). **R. White**: Conceptualization (equal); Supervision (equal); Writing – review & editing (equal). **G. Vamvounis**: Conceptualization (equal); Supervision (equal); Writing – review & editing (equal). **P. L. Burn**: Conceptualization (equal); Supervision (equal); Writing – review & editing (equal). **B. Philippa**: Conceptualization (equal); Supervision (equal); Writing – original draft (equal); Writing – review & editing (equal).

DATA AVAILABILITY

The data that support the findings of this study are available within the article and its supplementary material.

REFERENCES

[1] N. C. Giebink and S. R. Forrest, "Quantum efficiency roll-off at high brightness in fluorescent and phosphorescent organic light emitting diodes," Phys. Rev. B **77**(23), 235215 (2008).
[2] C. Murawski, K. Leo, and M. C. Gather, "Efficiency roll-off in organic light-emitting diodes," Adv. Mater. **25**(47), 6801–6827 (2013).
[3] M. A. Baldo, C. Adachi, and S. R. Forrest, "Transient analysis of organic electrophosphorescence. II. Transient analysis of triplet-triplet annihilation," Phys. Rev. B **62**(16), 10967–10977 (2000).
[4] S. Reineke, K. Walzer, and K. Leo, "Triplet-exciton quenching in organic phosphorescent light-emitting diodes with Ir-based emitters," Phys. Rev. B **75**(12), 125328 (2007).
[5] H. van Eersel, P. A. Bobbert, R. A. J. Janssen, and R. Coehoorn, "Effect of Förster-mediated triplet-polaron quenching and triplet-triplet annihilation on the efficiency roll-off of organic light-emitting diodes," J. Appl. Phys. **119**(16), 163102 (2016).
[6] Y. Zhang, J. Lee, and S. R. Forrest, "Tenfold increase in the lifetime of blue phosphorescent organic light-emitting diodes," Nat. Commun. **5**(1), 5008 (2014).
[7] M. Bösing, C. Zimmermann, F. Lindla, F. Jessen, P. van Gemmern, D. Bertram, N. Meyer, D. Keiper, M. Heuken, H. Kalisch, and R. H. Jansen, "Introduction of innovative dopant concentration profiles to broaden the recombination zone of phosphorescent OVPD-processed organic light emitting diodes," MRS Online Proc. Lib. **1154**(1), 1105 (2009).
[8] V. Adamovich, M. Weaver, and J. Brown, U.S. patent no. 7,151,339 (30 January 2004).
[9] B. D. Chin, M. C. Suh, M.-H. Kim, S. T. Lee, H. D. Kim, and H. K. Chung, "Carrier trapping and efficient recombination of electrophosphorescent device with stepwise doping profile," Appl. Phys. Lett. **86**(13), 133505 (2005).
[10] B. D. Chin, S.-H. Lee, J. K. Kim, and C. H. Lee, Proc. SPIE **6333**, 633315 (2006).
[11] J. Lee, J.-I. Lee, K.-I. Song, S. J. Lee, and H. Y. Chu, "Influence of doping profile on the efficiency of blue phosphorescent organic light-emitting diodes," Appl. Phys. Lett. **92**(13), 133304 (2008).
[12] B. M. Lee, J. Kim, G. J. Yun, W. Y. Kim, and P. Mascher, "Study on hybrid blue organic light emitting diodes with step controlled doping profiles in phosphorescent emitting layer," Opt. Mater. **86**, 498–504 (2018).
[13] C. Tonnelé, M. Stroet, B. Caron, A. J. Clulow, R. C. R. Nagiri, A. K. Malde, P. L. Burn, I. R. Gentle, A. E. Mark, and B. J. Powell, "Elucidating the spatial arrangement of emitter molecules in organic light-emitting diode films," Angew. Chem., Int. Ed. **56**(29), 8402–8406 (2017).
[14] M. Gao, T. Lee, P. L. Burn, A. E. Mark, A. Pivrikas, and P. E. Shaw, "Revealing the interplay between charge transport, luminescence efficiency, and morphology in organic light-emitting diode blends," Adv. Funct. Mater. **30**(9), 1907942 (2020).
[15] B. Minaev, G. Baryshnikov, and H. Agren, "Principles of phosphorescent organic light emitting devices," Phys. Chem. Chem. Phys. **16**(5), 1719–1758 (2014).
[16] S. Sanderson, B. Philippa, G. Vamvounis, P. L. Burn, and R. D. White, "Understanding charge transport in $Ir(ppy)_3$:CBP OLED films," J. Chem. Phys. **150**(9), 094110 (2019).

[17]S. Sanderson, G. Vamvounis, A. E. Mark, P. L. Burn, R. D. White, and B. W. Philippa, "Unraveling exciton processes in Ir(ppy)$_3$:CBP OLED films upon photoexcitation," J. Chem. Phys. **154**(16), 164101 (2021).
[18]V. Ahmad, J. Sobus, M. Greenberg, A. Shukla, B. Philippa, A. Pivrikas, G. Vamvounis, R. White, S.-C. Lo, and E. B. Namdas, "Charge and exciton dynamics of OLEDs under high voltage nanosecond pulse: Towards injection lasing," Nat. Commun. **11**(1), 4310 (2020).
[19]S. Sanderson, B. Philippa, G. Vamvounis, P. L. Burn, and R. D. White, "Elucidating the effects of guest-host energy level alignment on charge transport in phosphorescent OLEDs," Appl. Phys. Lett. **115**(26), 263301 (2019).
[20]S. Sanderson, G. Vamvounis, A. E. Mark, P. L. Burn, R. D. White, and B. W. Philippa, "Understanding the performance differences between solution and vacuum deposited OLEDs: A computational approach," J. Chem. Phys. **156**(21), 214703 (2022).
[21]Y. C. Zhou, L. L. Ma, J. Zhou, X. M. Ding, and X. Y. Hou, "Effect of a sensing layer on triplet exciton diffusion in organic films," Phys. Rev. B **75**(13), 132202 (2007).
[22]M. A. Lampert and P. Mark, *Current Injection in Solids* (Academic Press, 1970).
[23]N. D. Nguyen, M. Schmeits, and H. P. Loebl, "Determination of charge-carrier transport in organic devices by admittance spectroscopy: Application to hole mobility in α-NPD," Phys. Rev. B **75**(7), 075307 (2007).
[24]J.-W. Kang, S.-H. Lee, H.-D. Park, W.-I. Jeong, K.-M. Yoo, Y.-S. Park, and J.-J. Kim, "Low roll-off of efficiency at high current density in phosphorescent organic light emitting diodes," Appl. Phys. Lett. **90**(22), 223508 (2007).
[25]N. Chopra, J. Lee, Y. Zheng, S.-H. Eom, J. Xue, and F. So, "High efficiency blue phosphorescent organic light-emitting device," Appl. Phys. Lett. **93**(14), 143307 (2008).
[26]H. Park, D.-S. Shin, H.-S. Yu, and H.-B. Chae, "Electron mobility in tris(8-hydroxyquinoline)aluminum (Alq_3) films by transient electroluminescence from single layer organic light emitting diodes," Appl. Phys. Lett. **90**(20), 202103 (2007).
[27]G. G. Malliaras, Y. Shen, D. H. Dunlap, H. Murata, and Z. H. Kafafi, "Nondispersive electron transport in Alq_3," Appl. Phys. Lett. **79**(16), 2582–2584 (2001).
[28]M. Kleinschmidt, C. van Wüllen, and C. M. Marian, "Intersystem-crossing and phosphorescence rates in fac-Ir^{III}(ppy)$_3$: A theoretical study involving multi-reference configuration interaction wavefunctions," J. Chem. Phys. **142**(9), 094301 (2015).
[29]S. Reineke, G. Schwartz, K. Walzer, and K. Leo, "Direct observation of host–guest triplet–triplet annihilation in phosphorescent solid mixed films," Phys. Status Solidi RRL **3**(2–3), 67–69 (2009).
[30]S. Tokito and I. Tanaka, "Phosphorescent organic light-emitting devices: Triplet energy management," Electrochemistry **76**(1), 24–31 (2008).
[31]C. Adachi, R. Kwong, and S. R. Forrest, "Efficient electrophosphorescence using a doped ambipolar conductive molecular organic thin film," Org. Electron. **2**(1), 37–43 (2001).